Fractal flame structure due to the hydrodynamic Darrieus-Landau instability

Rixin Yu,[1,*] Xue-Song Bai,[1] and Vitaly Bychkov[2,†]
[1]*Division of Fluid Mechanics, Department of Energy Sciences, Lund University, 22100 Lund, Sweden*
[2]*Department of Physics, Umeå University, SE–901 87, Umeå, Sweden*
(Received 3 August 2015; published 28 December 2015)

By using large scale numerical simulations, we obtain fractal structure, which develops at originally planar flame fronts due to the hydrodynamic Darrieus-Landau (DL) instability bending the fronts. We clarify some important issues regarding the DL fractal flames, which have been debated for a long time. We demonstrate an increase of the flame propagation speed with the hypothetic channel width, which controls the length scale of the instability development. We show that this increase may be fitted by a power law indicating the mean fractal properties of the flame front structure. The power exponent in this law is found to be not a universal constant, rather it depends on the flame properties—on the density drop at the front. Using box counting on the simulated flame front shapes we show the fractal flame dimension at the intermediate scale is smaller than the one given by the power law, but it has a similar dependency on the density drop. We also obtain a formation of pockets at the DL fractal flame fronts, which previously has been associated only with turbulent burning.

DOI: 10.1103/PhysRevE.92.063028 PACS number(s): 47.70.Pq, 47.20.Ma

I. INTRODUCTION

The Darrieus-Landau (DL) instability of deflagration (flame) fronts is one of the most fascinating and important hydrodynamic phenomena emerging in combustion [1,2], inertial confinement fusion [3–5], and thermonuclear supernovae [5–7]. The DL instability develops because of the density drop (expansion of the burning gas) at a flame front described by the ratio of the unburned fuel/oxidizer mixture to the burnt gas density, $\Theta = \rho_f/\rho_b$. Due to the gas expansion, a propagating flame modifies the gas flow, which leads to unstable spontaneous wrinkling of an originally smooth front. Recently, instabilities with similar properties have also been obtained for transformation fronts in advanced materials—organic polymer semiconductors (doping fronts) [8,9] and crystals of nanomagnets (spin-avalanches) [10,11]. For the advanced materials, the electric and magnetic fields play conceptually the same role as the gas flow field in combustion, which demonstrates the fundamental importance and universality of the DL instability in Nature.

The nonlinear outcome of the DL instability has been actively debated for more than 70 years [1,2]. First, it was supposed that the DL instability makes burning intrinsically turbulent. Later, an opposite scenario has been favored that strong linear (thermal) and nonlinear (Huygens) stabilization of the DL instability leads to smooth cellular flame structure as illustrated in Fig. 1(a) with some—relatively minor—increase of the flame propagation speed [12–16]. As a new turn in the debate, analysis of the experimental data [17] demonstrated self-accelerative growth of the expanding flame ball radius at sufficiently large length scales, $R \propto t^{\alpha}$, $\dot{R} \propto R^{d}$, with $\alpha = 1/(1-d)$. The acceleration had been interpreted as the emergence of the fractal flame structure with a cascade of front cells of different sizes imposed one on another. Reference [17] found $d \approx 1/3$, treated it as excess of the fractal flame dimension over the embedding dimension (the total front dimension is then $2+d$), and assumed that d was a universal constant. Since the velocity of Kolmogorov turbulence depends on the length scale in a similar way, $u_{turb} \propto l^{1/3}$, then the development of the DL fractal flames was also treated as spontaneous flame turbulization [17]. However, later refined experiments [18–20] reported a considerable spreading of the value d for flames with different properties in different fuel mixtures, see also [21,22] for similar experiments in tubes. We point out that accurate experimental measurements of d are complicated by the influence of gravity, confinement, flame-acoustic interaction, etc. Thus, the question about the DL fractal flame parameter d persisted; it was not even clear if this value is a universal constant or it depends on flame properties.

On the theoretical side, in spite of active research, an understanding of the DL fractal flames is still in its infancy. Most of the theoretical works on the subject have been performed in the scope of the simplified models of the Sivashinsky equation and its coordinate-free counterpart, e.g., see [23–26] and the review [13] for early references. Unfortunately, these two models are limited to the domain of small gas expansion, $\Theta - 1 \ll 1$, quite unrealistic for combustion experiments, and yield contradictory results. After proper re-scaling, the Sivashinsky equation does not contain the density drop Θ and, hence, any theoretical study of fractal flames by this method assumes *a priori* that the fractal parameter d (if any) is a universal constant. On the contrary, Ref. [26] argued that the Sivashinsky equation is too oversimplified to describe fractal flames and, by employing the coordinate-free model, demonstrated that d depends strongly on the density drop Θ as $d \propto (\Theta-1)^2$ for $\Theta - 1 \ll 1$. Attempts to reproduce fractal flame properties in direct numerical simulations were not successful either so far because of too large flow scales and too large numerical resources required for that purpose [27–29]. These works either came marginally close to the expected domain of the DL fractal flames or did not resolve the flame structure properly, which made the results unreliable. Thus, the theoretical works on the subject performed up to now did not answer the main questions posed by the experiments; the purpose of the present work is to overcome this shortcoming.

*rixin.yu@energy.lth.se
†Deceased.

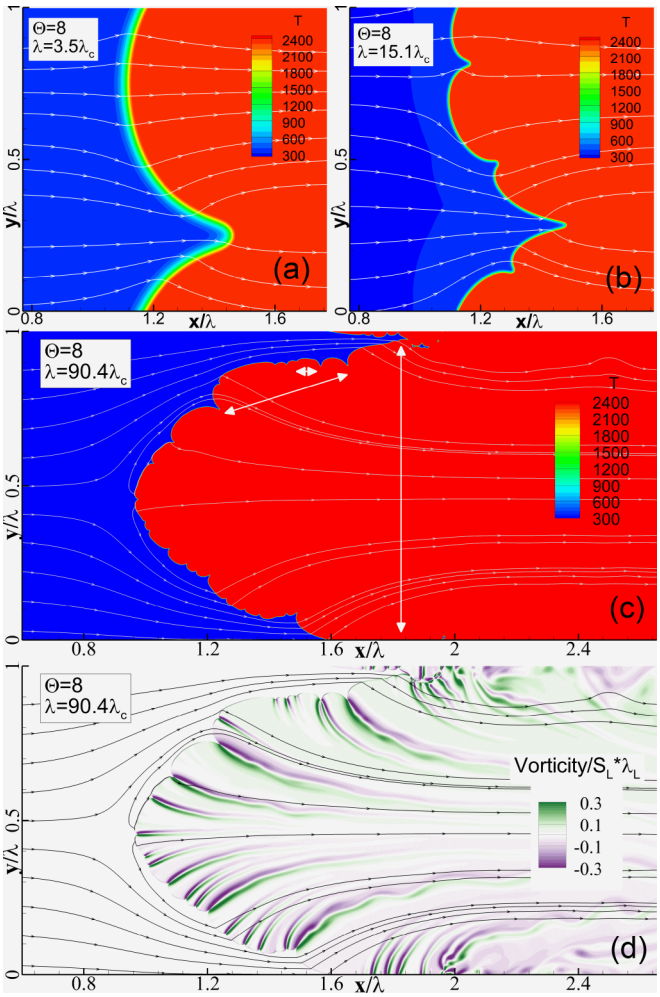

FIG. 1. (Color online) Characteristic snapshots of temperature distribution for a flame front with $\Theta = 8$ in a "channel" of width $\lambda = 3.5\lambda_c$ taken at $t = 5\lambda/S_L$ (a); $\lambda = 15.1\lambda_c$ at $t = 4.8\lambda/S_L$ (b); $\lambda = 90.4\lambda_c$ at $t = 1.9\lambda/S_L$, the white arrows indicate characteristic steps in the fractal cascade (c); vorticity distribution for $\lambda = 90.4\lambda_c$ at $t = 1.9\lambda/S_L$ (d).

Here we perform numerical simulations to obtain the DL fractal flame structure; the simulation results answer the most important fundamental questions raised by the experiments. To be specific, we consider an initially planar flame front propagating in a hypothetic "channel" of width λ with periodic boundary conditions at the "walls", which determine the spectrum of allowed perturbation wavelengths at the linear DL instability stage. A great advantage of the channel geometry for the problem of the DL fractal flames as compared to the geometry of expanding flames is in the possibility of obtaining stationary and statistically stationary flame propagation, as well as in better control of the flame dynamics.

II. GOVERNING EQUATIONS AND NUMERICAL METHODS

The DL stability is studied by solving the Navier-Stokes equations of low Mach number approximation with a one-step Arrhenius reaction in an ideal gas mixture. The governing equations are as follows:

$$\frac{\partial \rho}{\partial t} + \frac{\partial}{\partial x_j}(\rho u_j) = 0, \tag{1}$$

$$\frac{\partial}{\partial t}(\rho u_i) + \frac{\partial}{\partial x_j}(\rho u_j u_i + \delta_{ij} p - \sigma_{ij}) = 0, \tag{2}$$

$$C_v \frac{\partial}{\partial t}(\rho T) + C_p \frac{\partial}{\partial x_j}\left(\rho u_j T - \frac{\eta}{Pr}\frac{\partial}{\partial x_j} T\right) = Q \frac{\rho Y}{\tau_R} \exp\left(-\frac{E}{T}\right), \tag{3}$$

$$\frac{\partial}{\partial t}(\rho Y) + \frac{\partial}{\partial x_j}\left(\rho u_j Y - \frac{\eta}{LePr}\frac{\partial}{\partial x_j} Y\right) = -\frac{\rho Y}{\tau_R} \exp\left(-\frac{E}{T}\right), \tag{4}$$

where Y is the fuel mass fraction, T is temperature. C_p and C_v are the specific heat capacity at constant pressure and volume, respectively. The viscous stress tensor is given by

$$\sigma_{ij} = \eta\left(\frac{\partial u_i}{\partial x_j} + \frac{\partial u_j}{\partial x_i} - \frac{2}{3}\delta_{ij}\frac{\partial u_k}{\partial x_k}\right). \tag{5}$$

Under low Mach number assumption the physical pressure is decomposed as a hydrodynamic component p and a thermodynamic component P. $P(=1$ bar) is used in the equation of state for perfect gas mixture, $P = \rho RT/m$, with the molecular weight $m = 0.029$ kg/mole and the universal gas constant $R = C_p - C_v$. The reaction is given by an Arrhenius equation with the activation energy E (in units of temperature) and a constant chemical time dimension $\tau_R = 10^{-9}$ s. The upstream fuel has a temperature of $T_f = 300$ K. The energy release is given as $Q = (\Theta - 1)T_f C_p$, with $C_p = 7R/(2m)$. The viscosity is $\eta = 1.82 \times 10^{-5}$ Ns/m^2 and Prandtl number is $Pr = 0.3$. The Lewis number is set to unity $Le = 1$. The scaled activation energy is kept constant as $E/(\Theta T_f) = 7$. For the case of $\Theta = 8$ the laminar flame speed S_L and the laminar flame thickness $L_f = \eta/(P_r \rho_f S_L)$ calculated by the Zeldovich-Frank-Kamenetski formulation are 0.563 m/s and 92.7 μm, respectively. The above parameter settings are based on the previous study [27].

The numerical solver is modified based on a low Mach number reacting flow solver [30] employing detailed transport coefficients calculations and with a stiff ordinary differential equation (ODE) solver for general chemical reaction mechanism, which was used in various combustion studies [31–33]. The spatial discretization is based on a sixth-order center difference scheme, except that a fifth-order weighted essentially non-oscillatory (WENO) scheme [34] is used for the convective terms in the energy equation (3) and the fuel mass fraction equation (4) to avoid unphysical numerical oscillations. The temporal advancement of the convection, diffusion, and reaction (CDR) problem in the original solver is implemented using an operator-splitting algorithm in which the chemistry calculation is performed using a stiff solver while freezing the contributions from the convection and diffusion terms. In this work the one step reaction is non-stiff, therefore the temporal integration of the whole CDR problem is performed by an explicit second-order Adams-Bashforth method. The time step satisfies both the Courant-Friedrichs-Lewy (CFL) condition and the diffusion stability constraint. The

pressure/velocity decoupling results in a variable-coefficient Poisson equation for the hydrodynamic pressure which is solved using a multigrid method [36]. The numerical solver was implemented on staggered Cartesian grid of general space dimensions. The overall accuracy in space (fifth order) and time (second order) was verified by grid dependency tests.

The computing domain is a 2D rectangle of $x \in [0, L_x]$, $y \in [0, L_y]$ with $L_x/3 = L_y = \lambda$. The upstream fuel has a uniform inflow speed equal to the laminar flame velocity S_L. The convective outflow condition [35] is used at outlet, i.e., $\partial\phi/\partial t + U_{\rm conv}\partial\phi/\partial n = 0$ for any variable ϕ. Here n is outlet normal direction, the convective velocity $U_{\rm conv}$ is independent of location and is determined by global mass conservation, i.e., to make the outflow mass fluxes minus the incoming mass flux equal to the changing rate of total mass over entire domain. During evolution of DL instability the flame fronts propagate upstream with an unsteady pace. To study long time flame evolution it is important to ensure that the computational domain always covers the entire flame front surface. This is achieved by placing the computing domain on a moving observation coordinate which follows the movement of the mean flame front. For a 2D channel case, the moving coordinate (t', x', y') relates to the fixed coordinate (t, x, y) by $t' = t$, $y' = y$, and $x' = x + \int_0^t S_m(t^*)dt^*$. The velocity of the moving coordinate S_m is adjusted to make the mean flame x-position (ξ) stay close to the domain center (at $0.4L_x$), with

$$\xi(t) = \frac{1}{L_y}\int_0^{L_y}\int_0^{L_x} Y(t,x,y)dxdy. \qquad (6)$$

Written on two successive time steps t^n and t^{n+1}, $S_m(t^{n+1}) = S_m(t^n) + (\xi(t^{n+1}) - 0.4L_x)/(t^{n+1} - t^n)$, starting with $S_m(0) = 0$.

It is straightforward to show [36] that the governing equations on a moving coordinate differ from the ones on a fixed coordinate only with the unsteady terms changed as $\frac{\partial}{\partial t}(\rho\phi) = \frac{\partial}{\partial t'}(\rho\phi) + S_m\frac{\partial}{\partial x'}(\rho\phi)$ for any variable ϕ. For the convenience of later discussions the moving coordinate will still be referred to as (t, x, y).

Initially we imposed a steady 1D laminar flame at the x-domain center; the perturbation is added through shifting the 1D profile by a superposition of sinusoidal functions of small amplitudes representing numerically white-noise. A fine resolution with cell size $\Delta x = \Delta y = L_f/4$ is used for all cases of $\lambda < 1024L_f$, which compares well with the resolution ($\Delta x = L_f/5$, $\Delta y \geqslant \lambda/40 \approx 2L_f$) used in a previous study [27] with maximum channel width $\lambda = 4.6\lambda_c$. For very large cases ($\lambda \geqslant 1024L_f$) a slightly coarser resolution ($3\Delta x = 2\Delta y = L_f$) is used to ease the computation demand. Two simulations performed for ($\Theta = 8, \lambda = 1280L_f$) using both resolutions did not show noticeable changes in results. With the above resolution the numerically computed 1D stationary flame speed is within 5% error of the analytic one obtained from the Zeldovich-Frank-Kamenetski formula.

III. RESULT DISCUSSION

We perform simulations for the wide range of channel widths $\lambda = (10\text{–}1600)L_f$ and for the density ratios $\Theta = 5; 8; 10$. To avoid any influence of the thermal diffusion effects we take the Lewis number equal to unity. For sufficiently narrow channels of width below a certain cut-off value λ_c the DL instability is suppressed by thermal conduction, and an initially planar flame front remains planar. Using the same methods as [13,15], here we obtain the cut-off wavelengths $\lambda_c/L_f = 19; 17; 16$ for $\Theta = 5; 8; 10$, respectively, in a good agreement with the previous results [13,15,16]. For channel width somewhat larger than the cut-off wavelength, $\lambda > \lambda_c$, but still comparable to it, $\lambda \sim \lambda_c$, we find the growth of perturbations, which bend the front into a stationary curved cell as shown in Fig. 1(a). Due to a larger surface area, a curved flame consumes more fuel mixture per unit time and propagates with speed U_w exceeding the planar flame speed S_L. Figure 2(a) presents the velocity increase and saturation with time to a terminal stationary value for $\lambda = 3.5\lambda_c$ and $\Theta = 8$. Numerical U_w is calculated as the instantaneous mean flame speed relative to quiescent upstream flow, i.e., $U_m = \frac{d}{dt}\xi - S_m$. The analytical theory predicts the terminal stationary flame speed depending on the channel width λ as [37,38]

$$U_w = S_L + 4U_m\frac{N\lambda_c}{\lambda}\left(1 - \frac{N\lambda_c}{\lambda}\right), \qquad (7)$$

where $N = \mathrm{Int}[\lambda/2\lambda_c + 1/2]$ and $U_m(\Theta)$ is the maximal velocity increase for which the analytical formula has been found in [38] as $U_m/S_L = \frac{1}{2}\Theta(\Theta-1)^2/(\Theta^3 + \Theta^2 + 3\Theta - 1)$. Equation (7) predicts that at large length scales $\lambda \gg \lambda_c$ the flame propagation speed tends to its limiting value $U_w = S_L + U_m$ as shown by the dotted lines in Fig. 3. This prediction is in stark contrast with the power law $U_w/S_L \propto (\lambda/\lambda_c)^d$ expected for the fractal flames. Still, on moderate length scales of about $1 < \lambda/\lambda_c < 7\text{–}8$, our numerical simulations reproduce the theoretical prediction (7) quite well, which is also in a good agreement with the previous results [15,27].

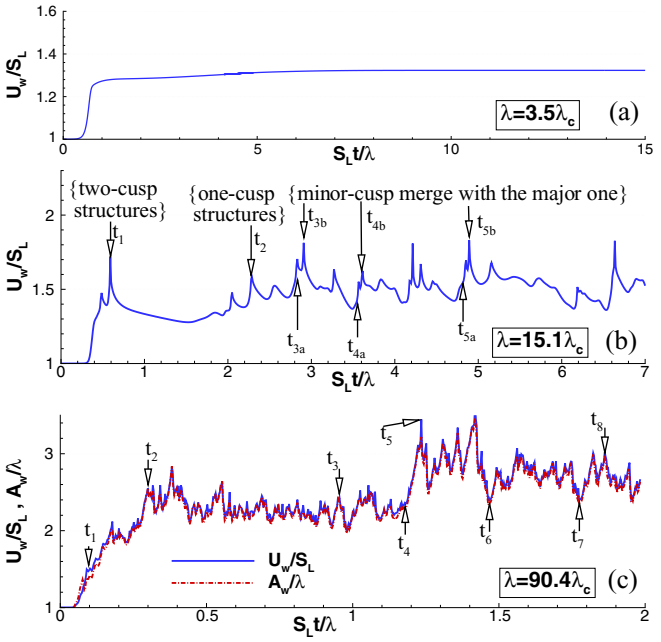

FIG. 2. (Color online) Scaled flame propagation speed U_w/S_L versus scaled time $S_L t/\lambda$ for a flame front with $\Theta = 8$ in a "channel" of width $\lambda = 3.5\lambda_c$ (a); $\lambda = 15.1\lambda_c$ (b); $\lambda = 90.4\lambda_c$ (c). The scaled length of the flame front A_w/λ is also shown in (c).

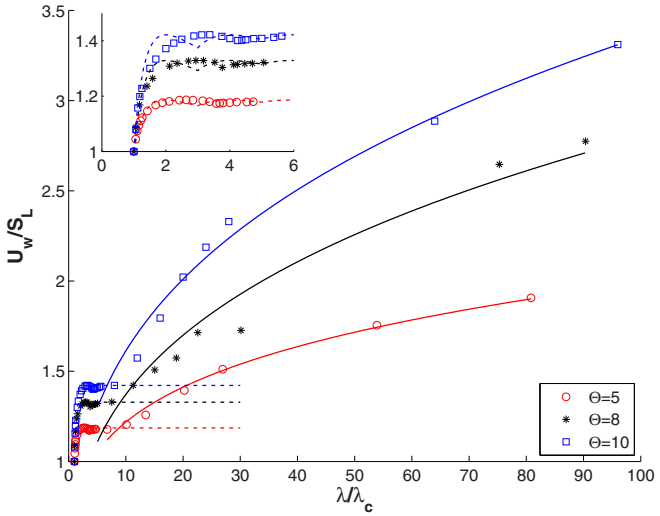

FIG. 3. (Color online) Terminal stationary or statistically stationary flame propagation speed U_w/S_L versus the scaled channel width λ/λ_c for $\Theta = 5; 8; 10$, with a zoomed insert. The dashed lines correspond to Eq. (7); the solid lines show the power law fit of the numerical data.

We obtain qualitatively new effects for channel widths exceeding the cut-off wavelength by order of magnitude, $\lambda/\lambda_c > 7-8$. In particular, Fig. 2(b) shows the time dependence of the scaled flame propagation speed U_w/S_L for $\Theta = 8$ and $\lambda = 15.1\lambda_c$. The evolution of the flame front shape is shown in Fig. 4(a) for eight selected time instants. In that case

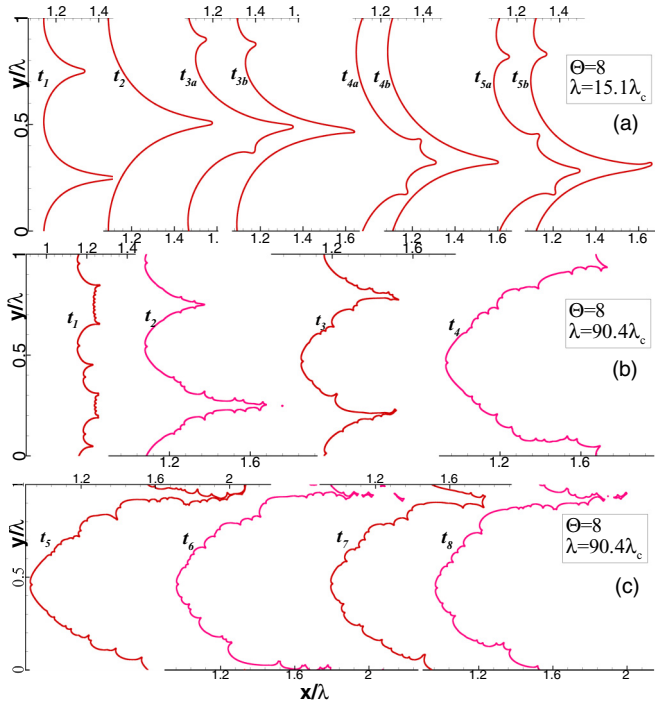

FIG. 4. (Color online) Time sequence of front evolution for two cases of $\Theta = 8$ with "channel" width $\lambda = 15.1\lambda_c$ (a) and $\lambda = 90.4\lambda_c$ (b and c). The time instants correspond to those marked in Fig. 2(b) and (c) (see Supplemental Material videos [41] for complete evolution at all three Θ with large channel width).

initial white-noise perturbations develop fast into a number of cells of a size about λ_c, which then coalesce forming a front structure with two long-living cusps (it corresponds to the first peak in the time dependence of U_w/S_L). Then, the two cusps merge into one, with the front structure resembling qualitatively Fig. 1(a). However, for a channel as wide as $\lambda = 15.1\lambda_c$, flame evolution does not stop at that point: after a while, smaller cusps arise spontaneously on the smooth parts of the front, move towards the larger cusp, and merge with the latter, in a statistically stationary manner, as shown by the front evolution from t_{3a} to t_{3b}, t_{4a} to t_{4b}, and t_{5a} to t_{5b} in Fig. 4(a). A characteristic flame shape in that process exhibits small cells imposed on larger ones as expected for fractal flames, as shown in Fig. 1(b). The same tendency becomes much more pronounced as we increase the channel width, see Fig. 1(c) for $\lambda = 90.4\lambda_c$; Fig. 1(d) depicts vorticity generation behind the corrugated flame front. In Fig. 1(c) we clearly recognize three successive steps in the fractal cascade as indicated by white arrows: one large cell of the size of the whole channel, 4–6 intermediate size cells imposed on the large one, and about 4–7 minor cells arising on the intermediate cells. The respective flame front evolution is shown in Fig. 4(b), (c). For a channel as wide as $\lambda = 90.4\lambda_c$ the process of arising and merging of intermediate and minor cusps becomes statistically stationary, see Figs. 2(c), 4(b), (c). In Fig. 2(c) we can also observe larger and smaller peaks in the flame propagation speed, with smaller peaks imposed on larger ones: these peaks correspond to merging of minor and intermediate flame cells, respectively.

In a sense, qualitatively similar (although much more simplified) evolution of the flame shape on large scales has been encountered previously in the Sivashinsky equation modeling [13,23–25]. Still, it is extremely important that minor cusps emerging at a curved flame in the Sivashinsky equation modeling did not produce additional increase of the flame propagation speed beyond the limiting value $U_w = S_L + U_m$ (unless external "turbulent" forcing was added to the equation). On the contrary, the present simulations indicate clearly that the fractal structure leads to considerable increase of the flame speed with the channel width, see Fig. 3. For example, for $\Theta = 8$ one has the limiting flame propagation speed $U_w \approx 1.3S_L$ as predicted by Eq. (7), but, at length scales as large as $\lambda = 90.4\lambda_c$, we find markedly higher statistically stationary flame propagation speed, $U_w \approx 2.5S_L$. Remarkably, similar to the case $\lambda = 15.1\lambda_c$, for $\lambda = 90.4\lambda_c$ we also observed first a long-living statistically quasi-stationary structure with two major cusps as an intermediate asymptotic before the two major cusps merged into one, see Fig. 4(b). The transition from a two-cusp to one-cusp structure was accompanied by a noticeable increase in the average flame propagation speed. Figure 2(c) shows also very good correlation between the flame propagation speed and the increase of the total length A_w of the wrinkled front, $U_w/S_L \approx A_w/\lambda$, which supports the classical model of an infinitely thin front propagating with the local speed S_L employed to understand the DL fractal flames [13,17]. In addition, Fig. 1(c) demonstrates that the fractal flame front cannot be described by a one-folded function $z = f(x,t)$ used as a basis for the Sivashinsky equation: the flame front in Fig. 1(c) is obviously multi-folded. Even more, we find that the fractal flame structure at sufficiently large

scales is accompanied by the formation of pockets of unburned fuel mixture in the burnt gas [see Figs. 1(c) and 4(c) at t_6 and t_8]; previously, such an effect has been associated with turbulent burning only. In the Barrere-Borghi diagram [2] the formation of pockets is typically employed as a sign for the transition from the regime of wrinkled to corrugated turbulent flames.

At sufficiently large channel widths $\lambda \gg \lambda_c$, the numerical data for the statistically stationary flame propagation speed may be fitted by a power law $U_w/S_L = C(\lambda/\lambda_c)^d$, where C is some constant and the power exponent d can be regarded as the fractal flame dimension similarly as [17,18] (the power-law curves are presented in Fig. 3 by the solid lines). We find the parameter d as $d \approx 0.213; 0.310; 0.318$ with $C \approx 0.67$–0.75 for the density drops $\Theta = 5; 8; 10$. Thus, the fractal parameter d is not a universal constant, but it depends on the density drop at the flame front, $d(\Theta)$, demonstrating a noticeable increase with Θ. At the same time, for the realistic values of the density drop, $\Theta = 5; 8; 10$, the parameter d remains rather close to $1/3$ in agreement with the experimental observations [17].

The above computed d relies on comparing the statistical stationary U_w from different channel widths, we may estimate another box-counting fractal parameter d' using the flame fronts from a single large channel width. In the box counting method [39] one covers a fractal curve image with square boxes and counts the number of boxes needed to cover the curve completely. Such a process is repeated with different box size. The slope of the log-log plot of the number of covering boxes verses the box size indicates the fractal parameter. The box counting method has been applied to study turbulent premixed flames [40]. Figure 5 shows the box-counting fractal dimension $1 + d'$ as a function of box size r for three density ratios at large channel width. Note λ_c limits the scale cascading from below. For intermediate box size $r \in [5\lambda_c, 24\lambda_c]$, $d' \approx 0.069; 0.104; 0.124$ at three density ratios $\Theta = 5; 8; 10$. The box-counting fractal parameter (d') is smaller than the power exponent (d); such difference can be explained by the large-scale single cusp shape of the flame front as shown in Fig. 4(c): the ratio of the cusp's depth to the width of the major cusp seems to be significantly larger than those for the intermediate and minor cusps. This suggests that the flame front area A_w (therefore U_w) receives more contributions from large scales than it would provide by a power-law scale dependence of constant exponent, which is also shown in Fig. 5 by the high d' at large scales. The power exponent d should therefore be regarded as a "mean" fractal parameter.

Albeit small, d' shows a similar trend of increasing with density ratio.

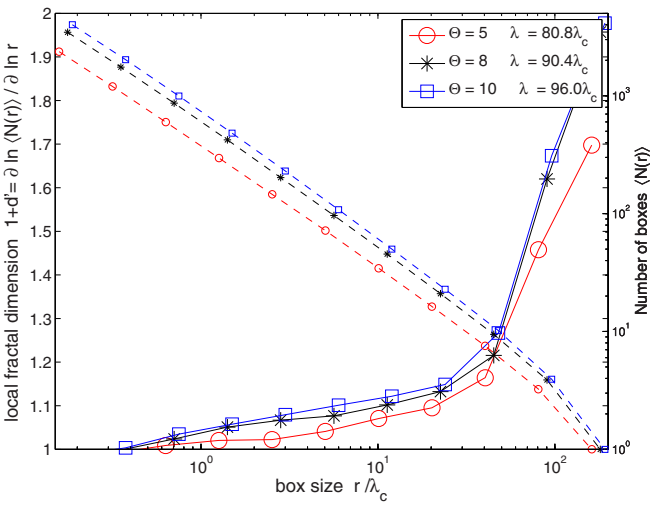

FIG. 5. (Color online) 2D box-counting the flame front images for three large channel cases at different density ratio $(\Theta,\lambda) = (5,80.8); (8,90.4); (10,96)$. With box size r, the box-counting fractal dimension (solid lines) is $1 + d' = \partial \ln \langle N(r) \rangle / \partial \ln r$, the dashed lines denotes $\langle N(r) \rangle$. $N(r)$ is a mean number of boxes covering one frame of flame front image, the bracket $\langle \cdot \rangle$ represents time average after statistical stationary structure of a single cusp shape forms, see Supplemental Material videos [41]. The frame sampling duration is about λ/S_L which covers many events of cusp formations. The counting is performed with a series of boxes of size $r_k = r_0 2^k$. Each frame image is binarized as a periodic square array of size 1024^2. To achieve better counting with a large box, one image frame has the array shifted circularly with a 32 interval to produce a 32^2 periodic variants of the same image.

IV. SUMMARY

As a summary, here we provide a reliable theoretical demonstration of the fractal flame structure developing owning to the DL instability. Our large scale numerical simulations clarify the important fundamental properties of the DL fractal flames. For sufficiently wide channels we demonstrate a power-law increase of the statistically stationary flame propagation speed with the channel width controlling the DL instability dynamics. We show that the power exponent d for characterizing a "mean" fractal flame dimension is not a universal constant, but it increases with the density drop Θ at the flame front. Box counting of the flame front shapes gives a lower fractal dimension at intermediate scale, which also increases with density drop.

ACKNOWLEDGMENTS

The authors gratefully acknowledge the financial support by the Swedish Research Council (Vetenskapsråde). We acknowledge PRACE for awarding us access to computer resource supermuc based in Germany at Leibniz-Rechenzentrum in Garching near Munich. Part of simulations were performed on resources provided by the Swedish National Infrastructure for Computing (SNIC) at Alarika cluster.

[1] L. D. Landau and E. M. Lifshitz, *Fluid Mechanics* (Pergamon Press, Oxford, 1989).

[2] C. K. Law, *Combustion Physics* (Cambridge University Press, Cambridge, 2006).

[3] M. Modestov, V. Bychkov, D. Valiev, and M. Marklund, Phys. Rev. E **80**, 046403 (2009).
[4] A. Piriz and N. Tahir, New J. Phys. **15**, 015013 (2013).
[5] V. Bychkov, M. Modestov, and C. K. Law, Prog. Energy Combust. Sci. **47**, 32 (2015).
[6] J. B. Bell, M. S. Day, C. A. Rendleman, S. E. Woosley, and M. Zingale, Astrophys. J. **606**, 1029 (2004).
[7] D. Kasen, F. K. Ropke, and S. E. Woosley, Nature **460**, 869 (2009).
[8] P. Matyba, K. Maturova, M. Kemerink, N. D. Robinson, and L. Edman, Nat. Mater. **8**, 672 (2009).
[9] V. Bychkov, P. Matyba, V. Akkerman, M. Modestov, D. Valiev, G. Brodin, C. K. Law, M. Marklund, and L. Edman, Phys. Rev. Lett. **107**, 016103 (2011).
[10] D. A. Garanin, Phys. Rev. B **88**, 064413 (2013).
[11] O. Jukimenko, C. M. Dion, M. Marklund, and V. Bychkov, Phys. Rev. Lett. **113**, 217206 (2014).
[12] P. Clavin, Prog. Energy Combust. Sci. **11**, 1 (1985).
[13] V. Bychkov and M. Liberman, Phys. Rep. **325**, 115 (2000).
[14] C. Clanet and G. Searby, Phys. Rev. Lett. **80**, 3867 (1998).
[15] V. V. Bychkov, S. M. Golberg, M. A. Liberman, and L. E. Eriksson, Phys. Rev. E **54**, 3713 (1996).
[16] S. Kadowaki, Phys. Rev. E **56**, 2966 (1997).
[17] Y. A. Gostintsev, A. G. Istratov, and Y. V. Shulenin, Combustion, Explosion, and Shock Waves **24**, 563 (1988).
[18] Y. A. Gostintsev, A. G. E. Istratov, N. I. Kidin, and V. E. E. Fortov, High Temperature **37**, 603 (1999).
[19] O. Kwon, G. Rozenchan, and C. K. Law, Proc. Comb. Inst. **29**, 1775 (2002).
[20] F. Wu, G. Jomaas, and C. K. Law, Proc. Combust. Inst. **34**, 937 (2013).
[21] J. Quinard, G. Searby, B. Denet, and J. Grana-Otero, Flow Turb. Combust. **89**, 231 (2012).
[22] C. Almarcha, B. Denet, and J. Quinard, Combust. Flame **162**, 1225 (2015).
[23] B. Galanti, O. Kupervasser, Z. Olami, and I. Procaccia, Phys. Rev. Lett. **80**, 2477 (1998).
[24] Y. D'Angelo, G. Joulin, and G. Boury, Combust. Theory Model. **4**, 317 (2000).
[25] V. Karlin and G. Sivashinsky, Proc. Combust. Inst. **31**, 1023 (2007).
[26] S. Blinnikov and P. Sasorov, Phys. Rev. E **53**, 4827 (1996).
[27] O. Y. Travnikov, V. V. Bychkov, and M. A. Liberman, Phys. Rev. E **61**, 468 (2000).
[28] M. Liberman, M. Ivanov, O. Peil, D. Valiev, and L.-E. Eriksson, Phys. Fluids **16**, 2476 (2004).
[29] S. Kadowaki, S. Suzuki, and H. Kobayashi, Proc. Combust. Inst. **30**, 169 (2005).
[30] R. Yu, J. Yu, and X. S. Bai, J. Comput. Phys. **231**, 5504 (2012).
[31] R. Yu and X. S. Bai, Combust. Flame **160**, 1706 (2013).
[32] H. Carlsson, R. Yu, and X. S. Bai, Intl J. Hydrog. Energy **39**, 20216 (2014).
[33] R. Yu, X. S. Bai, and A. N. Lipatnikov, J. Fluid Mech. **772**, 127 (2015).
[34] G. S. Jiang and C. W. Shu, J. Comput. Phys. **126**, 202 (1996).
[35] J. H. Ferziger and M. Peric, *Computational Methods for Fluid Dynamics* (Springer-Verlag, Berlin, 1996).
[36] R. Yu and X. S. Bai, Intl. J. Numer. Meth. Fluids **71**, 13 (2013).
[37] G. Joulin and P. Cambray, Combust. Sci. Technol. **81**, 243 (1992).
[38] V. Bychkov, Phys. Fluids **10**, 2091 (1998).
[39] B. B. Mandelbrot, *The Fractal Geometry of Nature* (W. H. Freeman, New York, 1982).
[40] E. Cintosun, G. Smallwood, and O. Gulder, *45th AIAA Aerospace Sciences Meeting and Exhibit* (AIAA, 2007), p. 1349.
[41] See Supplemental Material at http://link.aps.org/supplemental/10.1103/PhysRevE.92.063028 for front evolution videos at three density ratios with large channel width.